ACS OMEGA

Open Access

http://pubs.acs.org/journal/acsodf

Article

Optimizing Phosphopeptide Structures That Target 14-3-3ε in Cutaneous Squamous Cell Carcinoma

Seraphine Kamayirese, Sibaprasad Maity, Lynne M. Dieckman, Laura A. Hansen, and Sándor Lovas*

Cite This: *ACS Omega* 2024, 9, 2719−2729

Read Online

ACCESS | Metrics & More | Article Recommendations | Supporting Information

ABSTRACT: 14-3-3ε is involved in various types of malignancies by increasing cell proliferation, promoting cell invasion, or inhibiting apoptosis. In cutaneous squamous cell carcinoma (cSCC), 14-3-3ε is overexpressed and mislocalized from the nucleus to the cytoplasm where it interacts with the cell division cycle 25 A (CDC25A) and suppresses apoptosis. Hence, inhibition of the 14-3-3ε−CDC25A interaction is an attractive target for promoting apoptosis in cSCC. In this work, we optimized the structure of our previously designed inhibitor of the 14-3-3ε−CDC25A interaction, pT, a phosphopeptide fragment corresponding to one of the two binding regions of CDC25A to 14-3-3ε. Starting from pT, we developed peptide analogs that bind 14-3-3ε with nanomolar affinities. Peptide analogs were designed by shortening the pT peptide and introducing modifications at position 510 of the pT(502−510) analog. Both molecular dynamics (MD) simulations and biophysical methods were used to determine peptide binding to 14-3-3ε. Shortening the pT peptide from 14 to 9 amino acid residues resulted in a peptide (pT(502−510)) that binds 14-3-3ε with a K_D value of 45.2 nM. Gly to Phe substitution in position 510 of pT(502−510) led to further improvement in affinity (K_D: 22.0 nM) of the peptide for 14-3-3ε. Our results suggest that the designed peptide analogs are potential candidates for inhibiting 14-3-3ε−CDC25A interactions in cSCC cells and thus inducing their apoptosis.

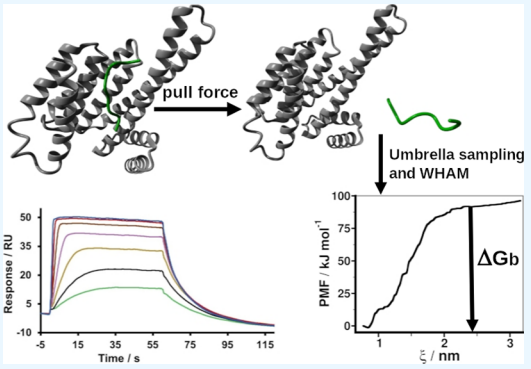

1. INTRODUCTION

14-3-3 proteins make up a family of highly conserved proteins that are expressed in all eukaryotic cells. In mammals, there are seven isoforms, β (when phosphorylated, β is called α) γ, ε, ζ (when phosphorylated, ζ is called δ), σ, η, and τ.[1−4] 14-3-3 proteins are biologically active in either homo- or heterodimeric forms, and the 14-3-3ε isoform only exists in the heterodimeric form.[5] Each monomer of 14-3-3 consists of nine antiparallel α-helices (αA, αB, αC, αD, αE, αF, αG, αH, and αI) (Figure 1). Helices αA, αB, and αD form the dimerization interface, while αC, αE, αG, and αI form an amphipathic ligand binding groove.[3,5−9] 14-3-3 proteins recognize a binding motif that contains phosphorylated amino acid residues. Although most binding partners of 14-3-3 have binding motifs containing phosphoserine (pSer),[2,10] the phosphorylated amino acid residue can also be threonine (pThr). FOXO, forkhead transcription factors,[11] aralkylamine N-acetyltransferase (AANAT),[12] and CDC25A[13,14] are some examples of 14-3-3 binding partners with pThr in their binding motifs. Yaffe and colleagues[2] used a pSer-oriented library to identify two consensus binding motifs, RSXpSXP and RXY/FxpSXP, that bind to all 14-3-3 isoforms. X denotes any type of amino acid residue, and pS is pSer.

The 14-3-3 proteins bind a plethora of proteins, thereby modulating cellular activities, such as cell cycle control, and apoptosis.[11,13−15] 14-3-3 proteins are associated with various pathological conditions, including neurodegenerative disorders like Parkinson's disease and Alzheimer's disease.[16] Further-

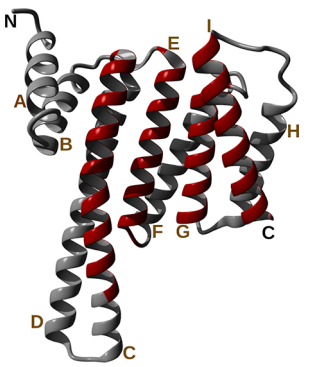

Figure 1. Ribbon representation of the monomeric structure of 14-3-3ε. Helices are labeled (A−I) from N- to C- terminal, and helices that form the binding groove are highlighted in red.

Received: October 5, 2023
Revised: December 13, 2023
Accepted: December 18, 2023
Published: January 3, 2024

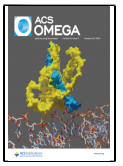

more, the 14-3-3 proteins are linked to various cancers, such as glioblastoma,[17] lung,[18] head and neck,[19] breast[20], and gastric[21] cancers. 14-3-3 proteins regulate oncoproteins and tumor suppressor proteins.[17−21] Studies have shown that the 14-3-3ε isoform is involved in various types of malignancies by increasing cell proliferation, invasion, or inhibiting apoptosis.[1,22] Likewise, increased expression of 14-3-3ε, and its mislocalization from the nucleus to cytoplasm, has been reported in cSCC, where it is associated with resistance to apoptosis.[14] In cSCC, 14-3-3ε forms heterodimers with γ and ζ isoforms.[23] Similar to 14-3-3ε, cell division cycle 25 A (CDC25A) is overexpressed in cSCC and inhibits apoptosis. This anti-apoptotic activity of CDC25A is dependent on its binding to a 14-3-3ε heterodimer at the region of pSer178 and/or pThr507 residues.[14,23,24] Thus, inhibition of the 14-3-3ε−CDC25A interaction is a promising target for the development of therapeutics for cSCC.

Efforts have been taken previously to control 14-3-3−ligand binding using different strategies, which include the use of 14-3-3−binding defective mutant, which negatively affects 14-3-3 mediated processes.[25] Moreover, peptide inhibitors of 14-3-3, such as R18 and difopein, have been used in functional studies[26] to prevent 14-3-3−ligand binding interactions. R18 is a 14-3-3 ligand isolated from a phage display library screen for peptide ligand for 14-3-3τ, but R18 also binds other 14-3-3 isoforms with high affinity.[26] The 14-3-3−R18 interaction is not dependent on phosphorylation, although X-ray structures[27] revealed that the Trp-Leu-Asp-Leu-Glu (residues 10−14) pentapeptide segment of R18 occupies the same amphipathic binding groove of 14-3-3 as a phosphopeptide does, and negatively charged residues Asp^{12} and Glu^{14} establish contacts similar to that of the pSer of phosphopeptides. R18 inhibits the interactions of 14-3-3 and its clients such as exoenzyme S,[28] Raf-1[26], and apoptosis signal-regulating kinase 1 (ASK1).[25] Difopein, a dimer of R18 peptide, also inhibits the 14-3-3−Raf-1 interaction, thus inducing apoptosis.[29] FOBISIN 101, a pSer/Thr mimetic small molecule, can block interactions of 14-3-3 with its clients, Akt and Raf-1. FOBISIN 101 also blocks the ability of 14-3-3 to activate exoenzyme S ADP-ribosyltransferase.[30]

MD simulations have been used to study 14-3-3 proteins and characterize their molecular interactions with their binding partners. Nagy and colleagues[7] revealed conformational changes of 14-3-3ζ in bound and apo states, as well as the binding mechanism of phosphopeptides to 14-3-3ζ. Using enhanced conformational sampling, Higo and colleagues[31] elucidated the binding process of phosphorylated myeloid leukemia factor 1 peptide to 14-3-3ζ and identified various interactions required for 14-3-3ζ−phosphopeptide binding. Furthermore, MD simulations of 14-3-3η−phosphopeptide complexes show the effect of phosphorylation on 14-3-3−ligand interactions and indicate interactions between the phosphate group of the peptides and basic amino acid residues of 14-3-3η.[32] Andrei and colleagues[33] also used MD simulation to rationally design high affinity stabilizers of 14-3-3 protein−protein interactions.

In the previous work by this group,[24] a novel, 14 amino acid residues peptide was designed, which corresponds to one of the two binding regions of CDC25A (Ac-CDC25A(502−515)-NH_2 (pT)) to 14-3-3ε. The peptide binds to 14-3-3ε, interrupts its interaction with CDC25A, and induces cell death of cSCC cells with an IC_{50} of 22.1 μM. In the current work, we optimize the structure of pT to improve its affinity for 14-3-3ε. Initially, we truncated the pT peptide to obtain its 9 amino acid residue analog, Ac-CDC25A(502−510)-NH_2 (pT(502−510)). Then, we modified pT(502−510) in position 510 to improve its binding affinity for 14-3-3ε. Here, we report peptide analogs that have binding affinities for 14-3-3ε that are higher than those of the original pT peptide.

2. MATERIALS AND METHODS

2.1. Molecular Dynamic Simulations. *2.1.1. Structure Preparation.* The 14-3-3ε−peptide complexes were generated from the previously studied 14-3-3ε−pT complex.[24] The 14 amino acid residues pT peptide was sequentially truncated to a 9 amino acid residue peptide pT(502−510) using the YASARA program[34] (Table S1). All of the designed peptides were *N*-terminally acetyl-protected and *C*-terminally amide-protected to maintain the electronic structure of the backbone as it is in CDC25A.

2.1.2. MD Simulations of 14-3-3ε−Peptide Complexes. MD simulations were carried out as described in ref 24, and GROMACS-2021 software package[35] was used with CHARMM36m force field.[36] The 14-3-3ε−peptide complex was solvated in TIP3 water molecules[37] in a rhombic dodecahedron with the minimal distance of the complex from the edge of the dodecahedron being 1.2 nm. The system was neutralized with Na^+ and Cl^- ions, and then the final concentration of NaCl was set to 150 mM. Then the system was subjected to 1000-step steepest descent energy minimization, followed by a 1 ns all-atom positionally restrained constant number of molecules and volume and temperature (NVT) simulation at 300 K using the velocity rescaling method;[38] the temperature was kept constant using the sd integrator with a time constant (τ_T) of 2.0 ps and integration time of 2 fs. Next, to ensure the system equilibration and relaxation, the system was subjected to 10 ns unrestrained simulation at a constant number of molecules, pressure, and temperature (NPT) at 300 K temperature and 1 bar pressure using the Berendsen methods.[39] With a 2 fs integration step, the Lincs algorithm[40] was used to constrain the hydrogen atoms to their correct length. The system was coupled to constant pressure by the Berendsen method[39] with an isothermal compressibility of 4.5×10^{-5} bar and to a 300 K temperature by velocity rescaling method with the stochastic term.[38] The time constants for pressure coupling (τ_p) and temperature coupling (τ_T) were 0.1 and 2 ps, respectively. To calculate the van der Waals interactions, the short-range cutoff was 1.0 nm and the long-range cutoff was 1.2 nm; a force switch modifier was used. The long-range electrostatic interactions were calculated using the PME method with a 1.2 nm cutoff distance with the Verlet scheme and 0.12 nm Fourier spacing. After equilibration, a 500 ns NPT simulation was performed with similar parameters as during equilibration, except that the system was coupled to a pressure using the Parrinello−Rahman barostat method[41] and the temperature was kept constant using stochastic dynamic integrator with τ_p and τ_T of 2 and 4 ps, respectively, and integration time of 2 fs.

2.1.3. Trajectory Analysis. To determine whether the system reached equilibration, configurational entropy was calculated.[42,43] The *covar* module of GROMACS was used to calculate the covariance matrix of the Cα-atoms movement, and eigenvectors corresponding to the 150 highest eigenvalues were used to calculate configurational entropy as a function of time.[43] To determine structural stability, the *rms* module of GROMACS was used to calculate C_α atoms root-mean-square

https://doi.org/10.1021/acsomega.3c07740
ACS Omega 2024, 9, 2719−2729

deviation (RMSD) for protein and the docked peptide.[44] The RMSD was calculated for the entire simulation trajectory, with reference to the initial structure. Changes in secondary structures of 14-3-3ε and peptides during simulations were analyzed using the defined secondary structure of proteins (DSSP) method.[45] To determine whether aromatic amino acid residues at position 510 of the peptides interact with residues of 14-3-3ε, representative structures of the last 100 ns of the simulations were determined using the GROMOS method of cluster analysis[44] with a C_α atom RMSD cutoff of 0.12 nm. Then, using the representative structure, the *distance* module of GROMACS was used to identify residues of 14-3-3ε that can interact with aromatic residues in position 510 of the peptides. The distance was calculated between the center of mass (COM) of side chain of residues of protein and COM of the ring of aromatic amino acid residue in position 510 of the peptides. 0.8 nm was used as the cutoff distance for interactions.[46,47]

2.1.4. Modifying pT(502−510) using FoldX. To generate various analogs of pT(502−510) peptide, FoldX[48,49] extension of the YASARA software was used to introduce modifications in the peptide. Here, five representative structures of 14-3-3ε−pT(502−510) complexes were obtained from the most populated clusters of five independent MD simulations. Guided by binding motifs of 14-3-3 proteins, modifications were made in the sequence of the pT(502−510) in each structure by substituting the amino acid residue of the peptide with different amino acid residues, one modification at a time (Table S2). The modifications were carried out at 310 K and pH 7.0. Change in free energy of binding ($\Delta\Delta G_b$) of 14-3-3ε to peptide due to modifications in the peptide was calculated using FoldX.[49]

2.1.5. Steered Molecular Dynamics (SMD) Simulations of 14-3-3ε−Peptide Complexes. For each amino acid modification, the structure that showed the most negative $\Delta\Delta G_b$, obtained by FoldX analysis, was used for the SMD simulations. The scheme of the SMD simulations is shown in Figure S4. 14-3-3ε−peptide complexes were solvated in TIP3 water molecules in a triclinic box with *x*, *y*, and *z* dimensions of 8.5, 9, and 13 nm, respectively. All the steps were carried out as described in the MD simulations section above, except that the system was equilibrated in a 100 ps NPT simulation so that the positions of Cα atoms are restrained in both protein and peptide with 400 kJ mol^{-1} nm^{-2} force constant. Then, the equilibrated system was subjected to a 4 ns SMD simulations.[50] Here, the position of heavy atoms of 14-3-3ε was fixed, and the COM of the peptide was pulled in the z direction (Figure S4) at a constant velocity of 1.0 nm ns^{-1} and a spring constant of 2500 kJ mol^{-1} nm^{-1}. The COM of the peptide was defined as the COM of the phosphorylated amino acid residue ($pThr^{507}$), while the COM of 14-3-3ε was defined as the COM of Lys,[50] Arg,[57] Arg^{130}, and Tyr^{131} residues[24] that interact with $pThr^{507}$.

2.1.6. Umbrella Sampling (US) Simulation. US simulations[50,51] were used to determine free energy of binding (ΔG_b) of the peptides to 14-3-3ε. Snapshots (24−27) from SMD simulations were used as starting configurations for US sampling. The snapshots were taken at every 0.1 nm of the COM distance between the protein and peptide (ξ reaction coordinate). A 4500 kJ mol^{-1} nm^{-2} umbrella potential was applied, and each window was simulated for 30 ns. Other parameters used here are the same as those in SMD simulations. Trajectories from the US simulation of each window were subjected to the weighted histogram analysis method (WHAM)[52,53] to obtain the potential of mean force (PMF). ΔG_b was determined from the PMF as the difference between the largest and smallest PMF values. Each PMF curve (Figure 4D) was obtained from a combination of histograms from five independent simulations during WHAM analyses. The errors were evaluated over 100 rounds of bootstrap analysis.

2.2. Protein. $(His)_6$-14-3-3ε was commercially obtained from Novus Biologicals (Centennial CO, USA), and 14-3-3ε-$(His)_{12}$ was expressed in our laboratory (see details on protein expression in the Supporting Information). The 14-3-3ε was expressed as a *C*-terminal His_{12}-tagged protein in *E. coli* BL21 (DE3) by induction with IPTG. The cells were harvested and lysed by sonication in lysis buffer (20 mM Tris, 200 mM NaCl, 20 mM imidazole, 1 mM DTT, pH 7.4), the cell lysate was centrifuged, and the supernatant was concentrated using a 10,000 Da MWCO Amicon spin filter by centrifuging at 4,000 rpm at 4 °C. The protein was initially purified by immobilized metal affinity chromatography (IMAC) using a HisTrap column (GE HealthCare, HisTrap FF Crude histidine-tagged protein purification columns). The column was equilibrated with 20 mM Tris, 200 mM NaCl, 20 mM imidazole, 1 mM DTT, pH 7.4 buffer. The protein was eluted with an imidazole gradient of 20 to 500 mM at a flow rate of 0.5 mL/min. The pooled fractions were concentrated into 20 mM Tris, 150 NaCl, 1 mM DTT, pH of 7.4 buffer using 10,000 Da MWCO Amicon spin filter and centrifuging at 4,000 rpm at 4 °C. The protein was further purified by size exclusion chromatography (SEC) using a superdex 75 column (Cytiva, superdex 75 increase 10/300 GL). The protein was eluted with the same buffer at a flow rate of 0.5 mL/min. The purified protein was stored at −80 °C.

2.3. Peptides. Peptides were either synthesized or commercially obtained from Biosynth International Inc. (Louisville KY, USA). All N-α-Fmoc-protected amino acids were obtained from CEM Corporation (Matthews NC, USA). Peptides were synthesized using standard Fmoc chemistry with Bzl, Boc, tBu, and Pbf side chain protections. The peptides were synthesized in 0.1 mmol scale on Rink amide resin using a CEM Discover microwave peptide synthesizer. Fmoc deprotection was performed using 20% piperidine in DMF for 2 min, and couplings were performed using DIC/Oxyma pure for 3 minutes at 75 °C. Single coupling cycles were performed for all amino acids, except double coupling for pThr. Peptides were cleaved from the resin and simultaneously deprotected by stirring it in a cocktail containing TFA/Thioanisol/TIPS/H_2O/DODT in 85:5:2.5:2.5:5 (v/v/v/v/v) for 1 h on ice and then 2 h at room temperature. The resin was then removed by filtration, and the peptide was precipitated with ice-cold diethyl ether and collected by filtration. The crude peptides were dissolved in 10% AcOH in H_2O and lyophilized. The crude products were purified by semi-preparative reversed-phase HPLC using a C18 column (Phenomenex, Jupiter 300 Å, 5 μm, 250 × 10 mm). The peptides were eluted using 0.1% TFA aqueous solution (v/v, solvent A) and 0.09% TFA in acetonitrile (v/v, solvent B) with a linear gradient of solvent B of 3 to 60% over 60 min, at a flow rate of 4 mL/min. The purity of the peptides was analyzed by analytical HPLC using the C18 (Jupiter 300 Å 5 μm, 250 × 4.6 mm) column, with the same gradient of solvent B over 40 min, at a flow rate of 1 mL/min. Masses of the peptides were

https://doi.org/10.1021/acsomega.3c07740
ACS Omega 2024, 9, 2719−2729

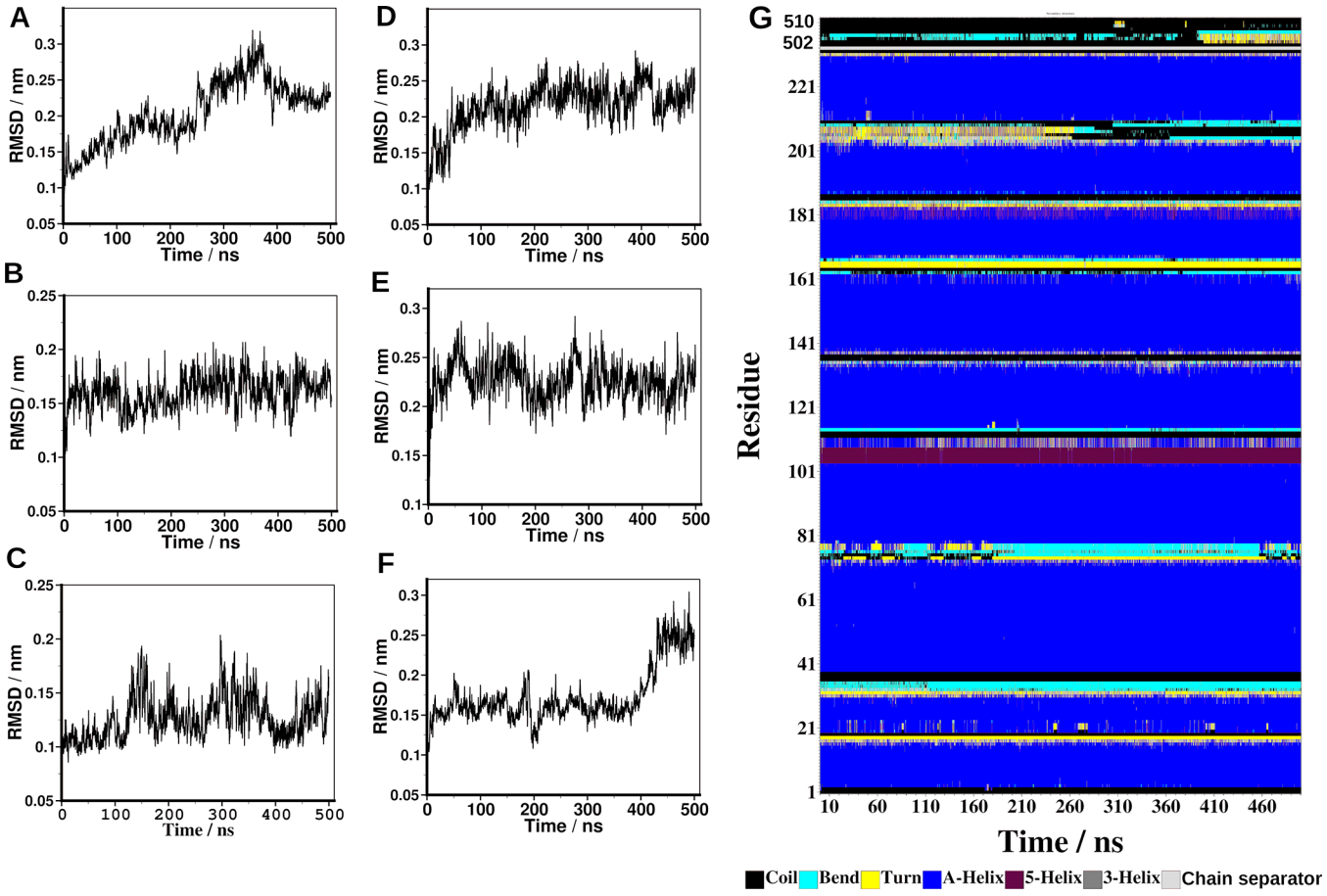

Figure 2. Root mean square deviations (RMSD) of Cα atoms and secondary structure of 14-3-3ε − peptide complexes. 14-3-3ε in complex with (A) pT(502−510). (B) [Phe^{510}]pT(502−510). (C) [Trp^{510}]pT(502−510). (D) [Tyr^{510}]pT(502−510). (E) [Ala^{510}]pT(502−510). (F) [Val^{510}]pT(502−510). (G) Change in the secondary structure of the 14-3-3ε−pT(502−510) complex during a 500 ns MD simulation. Secondary structure content was determined by the DSSP method.

determined by MALD-TOF mass spectrometry (Bruker, Billerica, MA, USA).

2.4. Electronic Circular Dichroism Spectropolarimetry. Peptides were dissolved in either nanopure water or 30, 50, and 75% (v/v) 2,2,2-trifluoroethanol (TFE) in water. Using a Jasco J-810 spectropolarimeter (Jasco Inc., Easton, MD), ECD spectra of the peptides were measured at 20 °C in a quartz cell with a 0.05 cm path length. ECD spectra of each peptide were obtained from an average of 20 scans from 180 to 260 nm at a rate of 100 nm/min. Mean residue ellipticity was calculated using peptide concentration determination using a NanoDrop One (Thermo Scientific) spectrophotometer at 280 nm wavelength. To quantify the secondary structure of the peptides, the ECD spectra were deconvoluted using the DichroWeb CD analysis web server and the CDSSTR method with reference set 6.[54,55]

2.5. Differential Scanning Fluorimetry (DSF). The melting temperature (T_m) of 14-3-3ε−peptide complexes was determined by DSF using the BioRad CFX384 Touch real-time PCR (Hercules CA, USA). The protein unfolding was detected with a fluorescent SYPRO-orange dye (Invitrogen). The assay was performed in 20 mM Tris, 150 mM NaCl, and 1 mM DTT PH7.4 buffer in a 386 well plate with a total volume of 20 μL, containing 2 and 30 μM, final concentrations of protein and peptide, respectively, and 500x dilution of the SYPRO-Orange dye stock from the manufacturer. The excitation filter for the dye was 450−490 nm, and the emission filter was 560−580 nm. The temperature was held at 25 °C for 5 min and then increased from 25 to 95 °C at a rate of 0.3 °C/min, and fluorescence was recorded over time. T_m values were determined by plotting the first derivative of the melting curve using GraphPad Prism software.

2.6. Surface Plasmon Resonance. Binding affinities of pT peptide analogs for 14-3-3ε were measured by SPR using a Biacore 8K Surface plasmon resonance instrument (Cytiva, Marlborough MA, USA). 100 nM 14-3-3ε-$(His)_{12}$ protein in 20 mM Tris, 150 mM NaCl, 50 μM EDTA, 0.005% Tween 20, pH 7.4 buffer was immobilized to a $NiCl_2$ activated NTA chip (Cytiva, Marlborough MA, USA) at a flow rate of 5 μL/min for 10 min and then washed with the running buffer for 20 min. Then peptide solutions at a concentration range of 1 nM−2000 nM were injected cycle-wise at the flow rate of 30 μL/min for 1 min, and dissociation time was set for 3 min. All SPR experiments were performed at 25 °C. The affinities and kinetics of the peptides binding to 14-3-3ε were determined by steady-state and 1:1 binding models, respectively, using Biacore Insight Evaluation Software (version 5.0.18.22102). At least three replicates were done for each peptide at similar conditions, and binding affinities (K_D) are presented as mean ± SD. K_D values were used to calculate binding free energy (ΔG) with the following formula: $\Delta G = RT \ln K_D$ (R = 1.986 cal mol^{-1} K^{-1}, T = 298 K).

https://doi.org/10.1021/acsomega.3c07740
ACS Omega 2024, 9, 2719−2729

3. RESULTS

3.1. Rational Design of pT Peptide Analogs. The Ac-CDC25A(502−515)-NH_2 (pT) binds to 14-3-3ε and induces death of cSCC cells with an IC_{50} of 22.1 μM.[24] Thus, here, we optimized the peptide structure to improve its binding affinity to 14-3-3ε. The proposed binding motifs of 14-3-3 proteins are defined by six to seven amino acid residues, RSXpSXP and RXY/FXpSXP.[2] Furthermore, X-ray structures of 14-3-3 in complex with various ligands showed that 14-3-3 proteins form complexes with short peptides.[56] Hence, to optimize the pT peptide, we sequentially truncated it from both the *N*- and *C*-termini (Table S1). The structures of truncated peptides in complexes with 14-3-3ε were studied by using 500 ns MD simulations. During simulations the complexes, protein, and peptides in the complexes went through various structural transitions as indicated by the RMSD of Cα atoms (Figure S1), but no peptide dissociation was observed for any peptide analogs. Since the short, 9 amino acid residue analog, pT(502−510) bound to 14-3-3ε (Figures 2A and S2), we used it for further analog design (detailed analysis of the simulation is given below).

Using the FoldX extension of the YASARA program, amino acid residues at different positions of pT(502−510) in the representative structures from five MD simulations (see methods) were replaced with various amino acids (Tables 1 and S2). Binding energies of the resultant peptides with 14-3-3ε were determined. Based on the binding motif of 14-3-3 proteins,[2] and the 14-3-3ε specific binding motif, RF/R/ARpSAPF,[10] either small hydrophobic, positively charged, or aromatic residues were introduced at positions that have been shown to be crucial for binding. Substitutions of Gly^{510} with aromatic amino acid residues were the most favorable among the modifications (Table 1). To find out if this is due to the aromaticity or hydrophobicity of the residues, we introduced hydrophobic aliphatic amino acid residues Ala and Val in position 510 as well. Although Gly^{510} to Phe modification resulted in the most favorable modification, constraining its side chain x^1 torsional angle can further improve the binding affinity of the peptide. Thus, Phe^{510} was replaced with 1,2,3,4-tetrahydroisoquinoline-3-carboxylic acid (Tic), an analog of Phe that is conformationally constrained in the x^1 torsional angle rotation[57] (Table 1 and Figure S6B). The binding of the designed peptides to 14-3-3ε was further studied using biophysical methods.

Table 1. Peptide Analogs of Ac-CDC25A(502-515)-NH_2 (pT) and the Change in Binding Energies upon Substituting Residue 510[a,b]

peptide	amino acid sequence	$\Delta\Delta G \pm$ SE/kJ mol^{-1}
pT	Ac-RTKSRpTWAGEKSKR-NH_2	
pT(502−510)	Ac-RTKSRpTWAG-NH_2	
[Phe^{510}]pT (502−510)	Ac-RTKSRpTWA*F*-NH_2	−5.06 ± 3.20
[Trp^{510}]pT (502−510)	Ac-RTKSRpTWA*W*-NH_2	−2.35 ± 1.94
[Tyr^{510}]pT (502−510)	Ac-RTKSRpTWA*Y*-NH_2	−6.18 ± 2.77
[Ala^{510}]pT (502−510)	Ac-RTKSRpTWA*A*-NH_2	1.45 ± 0.94
[Val^{510}]pT (502−510)	Ac-RTKSRpTWA*V*-NH_2	1.36 ± 1.61
[Tic^{510}]pT (502−510)	Ac-RTKSRpTWA*Z*-NH_2	N.D

[a]Modified residues are highlighted in italics. Changes in binding energies ($\Delta\Delta G_b$) between 14-3-3ε−peptide complexes were calculated using FoldX. The error was evaluated over $n = 5$ independent calculations and N.D: not determined. [b]Z, Tic; Ac, and $-NH_2$, acetyl and amide, respectively, protecting groups.

3.2. MD Simulations of Modified Peptides in Complex with 14-3-3ε. To determine whether the pT(502−510) and its designed analogs form stable complexes with 14-3-3ε, we carried out 500 ns MD simulations. Configurational entropy (Figure S2) shows that all systems experienced a steep decrease in the first 50 ns, followed by a gradual decrease between 50 ns and ∼300 ns, after which the systems reached equilibrium. RMSD of Cα-atoms as a function of time (Figure 2) shows that all peptides formed stable complexes with 14-3-3ε. 14-3-3ε-peptide complexes had RMSD between 0.1 and 0.3 nm. Complexes of 14-3-3ε with pT(502−510), [Tyr^{510}]pT(502−510), and [Val^{510}]pT(502−510) showed a gradual increase in RMSD, which became stabilized after 400 ns. Conversely, complexes containing [Phe^{510}]pT(502−510), [Trp^{510}]pT(502−510), and [Ala^{510}]-pT(502−510) showed a constant RMSD throughout the simulations (Figure 2). RMSDs of 14-3-3ε and the peptide separately, in all complexes, peptides showed larger RMSD than the 14-3-3ε (Figure S2). DSSP analysis of the 14-3-3ε − pT(502−510) complex showed that 14-3-3ε did not experience significant structural changes throughout the simulation. The peptide also maintained its structure with some coil to bent and turn transition of residues 504−506 in the last 150 ns of the simulation (Figure 2G). Both the protein and peptides maintained their structures in other protein−peptide complexes as well (Figure S3).

Having determined that aromatic amino acid residues are the most favorable substitutions in position 510 of pT(502−510), we identified 14-3-3ε amino acid residues that can interact with the aromatic amino acid residues in position 510 of the peptides. The following residues were identified within 0.8 nm of COM of the ring of Phe^{510}, Trp^{510}, and Tyr^{510} amino acid residue of peptides: Asn^{51}, Asn^{43}, Ser^{46}, Val^{47}, Phe^{120}, Lys^{123}, and Asp^{216} (Figure 3). Phe^{510} had the highest number of interacting residues within 0.8 nm of its COM compared to those of Trp^{510} and Tyr^{510} (Figure 3). The different types of amino acid residues of 14-3-3ε that were identified interact with the aromatic residues of the peptides through $\pi-\pi$, cation/anion−π, CH−π, and amide−π interactions.[46,47]

3.3. Binding Free Energy Analysis using the Umbrella Sampling Method. To determine $\Delta\Delta G_b$ of modified peptides with 14-3-3ε FoldX, we used one snapshot from an MD trajectory at a time. Therefore, to further assess binding of the peptides to 14-3-3ε, further MD simulations were performed. We first carried out SDM simulations, and then, snapshots from SMD trajectories were subjected to umbrella sampling simulations[50] and analyzed by the WHAM method.[52] Peptides were pulled away from the binding groove of 14-3-3ε by applying a force with a spring constant of 2500 kJ mol^{-1} nm^{-1} on the COM of the pThr507 residue of the peptides at a constant rate of 1 nm/ns. As shown by the force-time curve (Figures 4A and S5), all peptides show a rupture event around 500 ps with a rupture force of 700−900 kJ mol^{-1} nm, except the [Trp^{510}]pT(502−510) peptide for which the rupture occurred around at 1000 ps. The distance−time curves show minimal change in distance between COM of 14-3-3ε and COM of peptide in the first 500 ps and a gradual change over

https://doi.org/10.1021/acsomega.3c07740
ACS Omega 2024, 9, 2719−2729

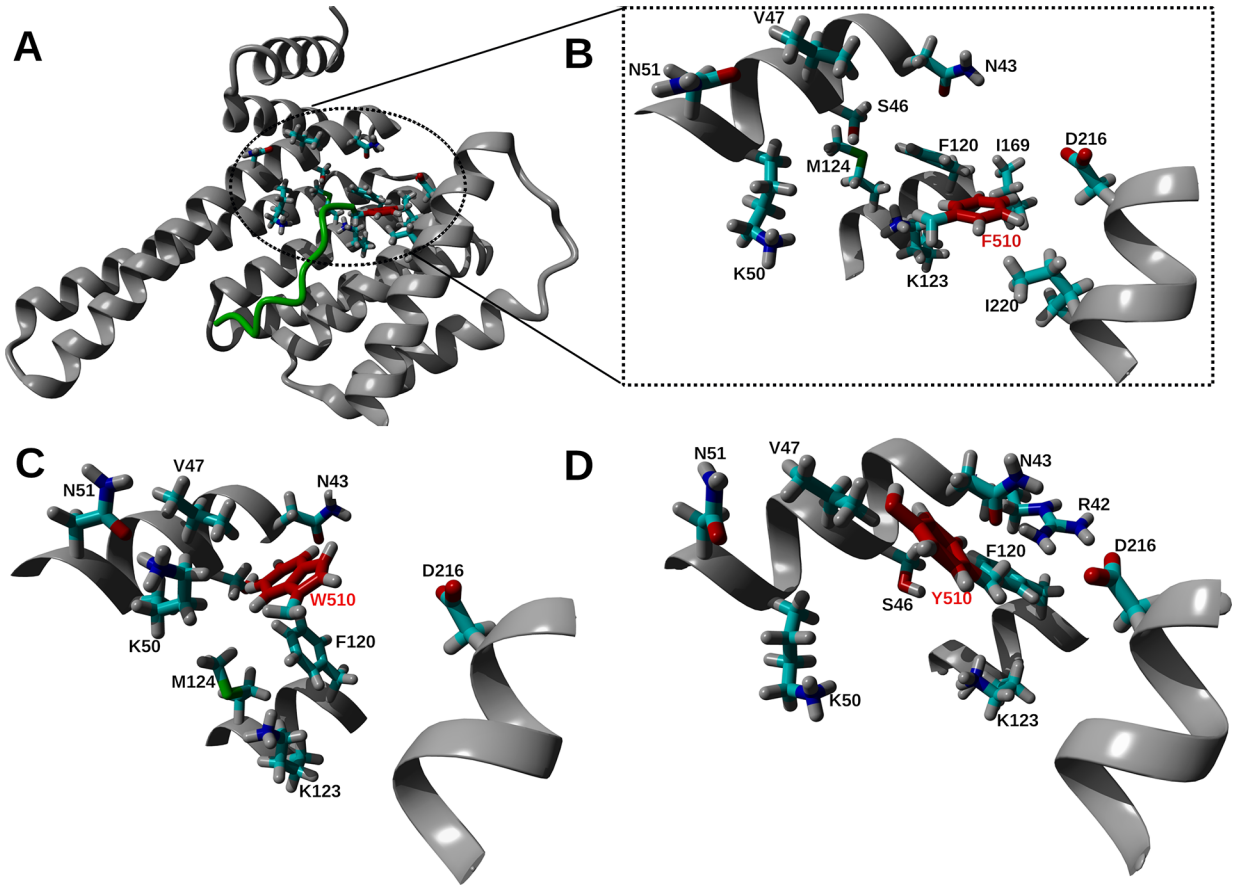

Figure 3. Interacting residues in the 14-3-3ε−peptide complexes. The structures of 14-3-3ε and [Phe^{510}] pT(502−510) peptide are shown as gray ribbon and green stick, respectively. Residues of 14-3-3ε that are within 0.8 nm of center of mass (COM) of the ring of aromatic amino acid residues in position 510 of peptides are in colored sticks. Amino acid residues are indicated in one letter code. The aromatic residue in position 510 of the peptide are shown by red sticks. Representative structures from 500 ns simulations were used. (A) Structure of 14-3-3ε−[Phe^{510}] pT(502−510) complex showing residues of the protein identified within 0.8 nm from COM of Phe^{510} of the peptide. (B,C,D) Close-up view of the identified amino acid residues when 14-3-3ε is in complex with [Phe^{510}] pT(502−510), [Trp^{510}] pT(502−510), and [Tyr^{510}]pT(502−510) peptides, respectively.

the rest of the simulation time (Figures 4B and S5), indicating a peptide dissociation after rupture. Curves in the US simulation histograms (Figure 4C) overlap, indicating that the simulations are well-suited for WHAM analysis. The PMF curves (Figure 4D) show that all peptides experienced a gradual increase in PMF up to the reaction coordinate (ξ) of ∼2 nm, after which the peptide dissociated from the protein; thus, PMF stayed constant. ΔG_b derived from PMF is shown in Figure 4E; all peptides favorably bound 14-3-3ε, as indicated by negative ΔG_b. The 14-3-3ε−pT(502−510) complex has a ΔG_b of −92.24 ± 6.56 kJ mol^{-1}. The 14-3-3ε−[Phe^{510}]pT-(502−510) formed a complex with the most negative ΔG_b, −143.99 ± 6.35 kJ mol^{-1}, while 14-3-3ε - [Val^{510}]pT(502−510) showed the lowest ΔG_b of −80.02 ± 5.47 kJ mol^{-1}. All other analogs formed complexes with ΔG_b in the range of −98.16 to −109.80 kJ mol^{-1}.

3.4. Structural Characterization of the Peptides. We used ECD spectropolarimetry to determine secondary structures of the peptide analogs dissolved in water and increasing TFE concentration. In water, the presence of a minimum at ∼198 nm suggests that the peptides adopted an unordered conformation,[58] and some of the peptides showed a spectral shift in the presence of TFE (Figures 5 and S7). To quantify the secondary structure content of the peptides, we analyzed ECD spectra using the CDSSTR method of the DichroWeb CD analysis server. The data (Table S3) show that the secondary structure of the peptides is a predominantly random coil with some helicity, β-stand, and β-turn conformations. In water, [Tic^{510}]pT(502−510) showed the most ordered structure regardless of TFE concentration. The structure of pT(502−510) was not affected by varying concentrations of TFE. Secondary structures of all other peptides became more structured in TFE, especially at 70% TFE. The parent pT peptide had the highest tendency to assume a more ordered structure with increasing TFE concentration (Figures 5 and S7 and Table S3).

3.5. Binding of pT Peptide Analogs to 14-3-3ε In Vitro. Based on MD simulation results, pT peptide analogs (Table 1) were either synthesized using Fmoc chemistry or commercially obtained from Biosynth Corporation. To confirm our computational results, we deciphered the binding of the synthetic peptides to 14-3-3ε by differential scanning fluorimetry (DSF). Figures 6 and S8 show the thermal unfolding profile of 14-3-3ε and the 14-3-3ε−pT(502−510) complex and their respective derivative curves. DSF results (Table 2) show that all peptides caused a shift in T_m (ΔT_m) of the 14-3-3ε, pT, and pT(502−510) peptides induced ΔT_m values of 2.43 ± 0.12 and 3.70 ± 0.06 °C, respectively. The [Phe^{510}]pT(502−510) caused the strongest ΔT_m of 5.19 ±

https://doi.org/10.1021/acsomega.3c07740
ACS Omega 2024, 9, 2719−2729

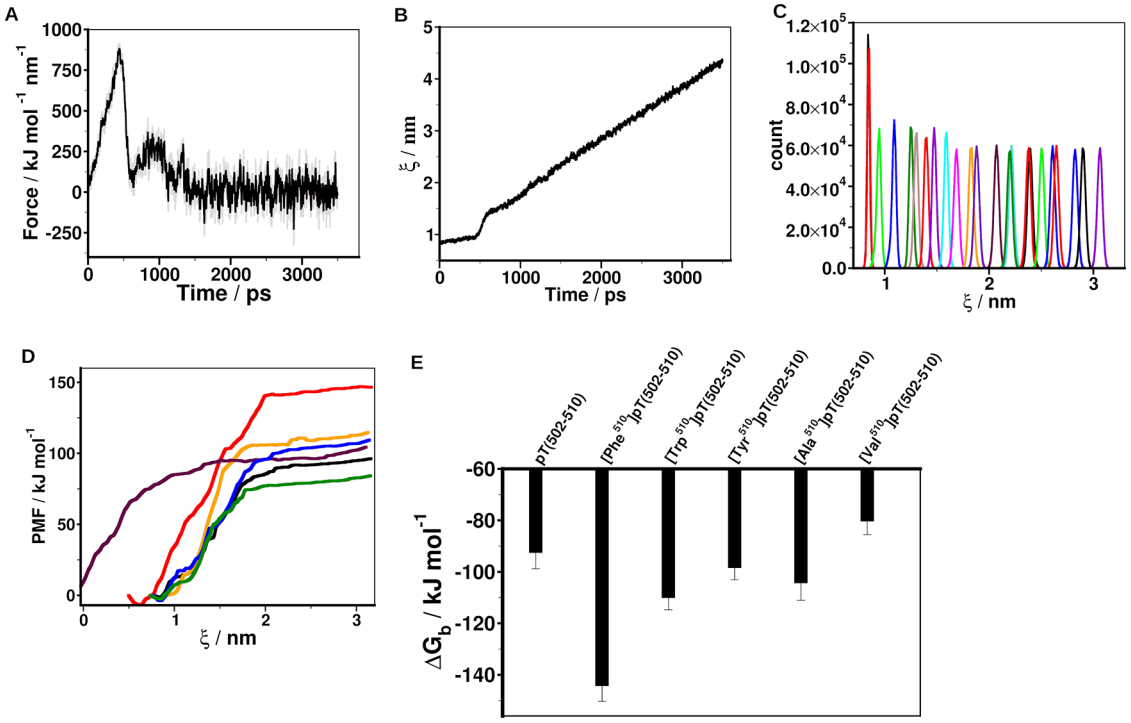

Figure 4. Steered molecular dynamics (SMD) simulations of 14-3-3ε−peptide complexes. (A) Time-dependent external force applied to pull pT(502−510) away from the binding groove of 14-3-3ε. (B) Time-dependent distance between the center of mass (COM) of 14-3-3ε and COM of pT(502−510). (C) Converged umbrella histograms of 27 configurations, each derived from 30 ns simulation of 14-3-3ε−pT(502−510). (D) Potential of mean force (PMF) curves obtained using the weighted histogram analysis method (WHAM). pT(502−510) (black), [Phe^{510}]pT(502−510) (brown), [Trp^{510}]pT(502−510) (orange), [Tyr^{510}]pT(502−510) (purple), [Ala^{510}]pT(502−510) (cyan), and [Val^{510}]-pT(502−510) (green). (E) Free energy of binding (ΔG_b) of 14-3-3ε−peptide complexes obtained from the potential of mean force (PMF). The free energies of binding were estimated as the difference between the maximum and minimum values of the PMF curves.

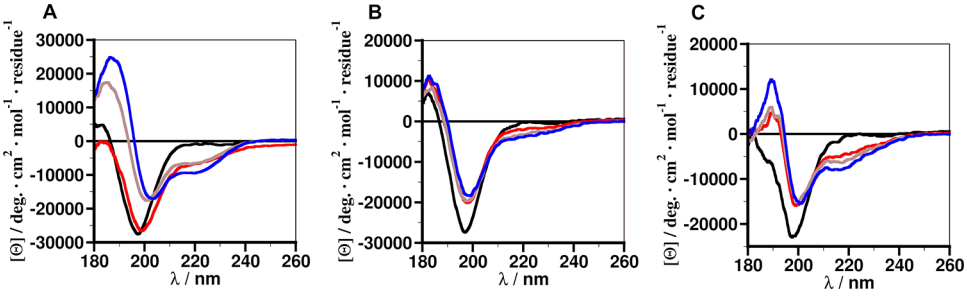

Figure 5. Electronic circular dichroism (ECD) spectra of peptides in different media. (A) pT; (B) pT(502−510); and (C) [Phe^{510}]pT(502−510). Black, water; red, 30% TFE; brown, 50% TFE; blue, 70% TFE. Each spectrum is an average of 20 scans. Mean residue ellipticity was determined from the concentration of the peptides.

0.41 °C, and other analogs led to ΔT_m in the range of 3.70−4.44 °C.

To quantify the binding affinity of the peptides to 14-3-3ε, we performed SPR and steady-state affinities (K_D) and kinetics of the peptides were determined. Representative sensorgrams are shown in Figures 7 and S8. As shown in Table 2, all the peptides had nanomolar binding affinity for 14-3-3ε, the pT peptide has a K_D value of 144.33 ± 2.5 nM, while pT(502−510) has a K_D value of 45.20 ± 24 nM. The kinetics (k_{on} and k_{off}) of the peptides are reported in Table S4 (K_D values calculated from the kinetics qualitatively reproduce the steady state affinities). Among all pT peptide analogs, [Phe^{510}]pT-(502−510) has the highest affinity for 14-3-3ε with a K_D of 22.0 ± 0.77 nM, while [Val^{510}]pT(502−510) has the weakest affinity for 14-3-3ε with a K_D of 211.66 ± 6.02 nM. The [Tic^{510}]pT(502−510) peptide had an affinity that is comparable to that of [Phe^{510}]pT(502−510). Free energy of binding (ΔG) derived from K_D shows that all peptides bound 14-3-3ε with a negative ΔG (Table 2).

4. DISCUSSION

In this work, by employing an array of different computational and experimental methods, we have shown that shortening and modifying the original pT peptide resulted in peptides with an improved affinity for 14-3-3ε (Table 2). 14-3-3ε is overexpressed and mislocalized to the cytoplasm in cSCC, and its interactions with CDC25A suppress apoptosis.[14] The previous study by our group[24] showed that pT peptide binds 14-3-3ε, inhibits its interaction with CDCC25A, and induces death of cSCC cells at a high concentration. Therefore, we aimed to improve the binding affinity of the peptide for 14-3-3ε, thus improving its activity against cSCC.

https://doi.org/10.1021/acsomega.3c07740
ACS Omega 2024, 9, 2719−2729

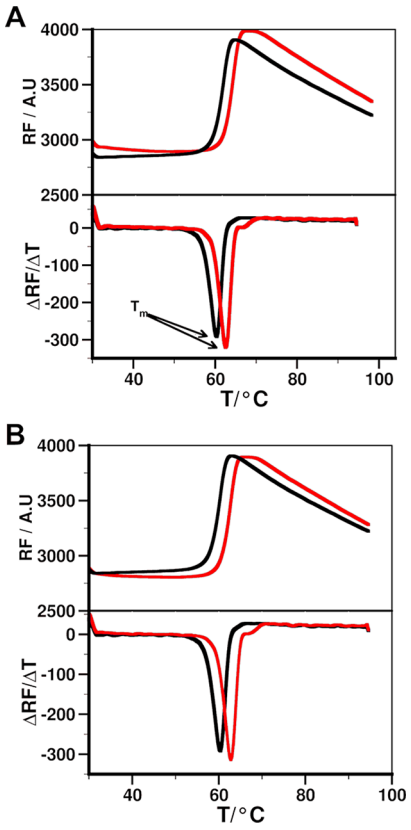

Figure 6. Binding of peptides to 14-3-3ε by differential scanning fluorometry (DSF). (A) Thermal denaturation of 14-3-3ε without (black) and with (red) peptide, and their respective first derivatives, from which melting temperature, T_m (inflection point of the curve), is determined; (A) pT; (B) pT(502−510). The presence of the peptide ligand shifts the black curve to the right. The degree of protein stabilization by the peptide can be calculated as a change in melting temperature (ΔT_m) between 14 and 3−3ε−peptide complex and 14-3-3ε.

Table 2. Melting Temperature Shift and Binding Affinity of Peptide Analogs for 14-3-3ε[a]

peptide	ΔT_m/°C	$K_D \pm$ SD/nM	$\Delta G \pm$ SD/kcal mol^{-1}
pT	2.43 ± 0.12	144.33 ± 2.5	−9.32 ± 0.01
pT(502−510)	3.70 ± 0.06	45.20 ± 24	−10.06 ± 0.29
[Phe^{510}]pT (502−510)	5.19 ± 0.41	22.0 ± 0.77	−10.42 ± 0.02
[Trp^{510}]pT (502−510)	3.70 ± 0.23	76.2 ± 12.60	−9.71 ± 0.10
[Tyr^{510}]pT (502−510)	3.78 ± 0.32	93.10 ± 4.57	−9.58 ± 0.029
[Ala^{510}]pT (502−510)	4.44 ± 0.48	75.37 ± 10.15	−9.71 ± 0.08
[Val^{510}]pT (502−510)	3.76 ± 0.38	211.66 ± 6.02	−9.12 ± 0.02
[Tic^{510}]pT (502−510)	4.43 ± 0.08	30.85 ± 0.18	−10.23 ± 0.02

[a]Change in melting temperature (ΔT_m) due to peptides binding to 14-3-3ε, and steady-state affinities (K_D) of peptides for 14-3-3ε were determined by DSF and SPR, respectively. ΔT_m values correspond to the average and SD of $n \geq 5$, and K_D values correspond tot the average and SD of $n \geq 3$. The free energies of binding (ΔG) were calculated from K_D.

We designed peptide analogs of pT and studied their binding to 14-3-3ε using MD simulations, DSF, and SPR. Our approaches to optimization of the pT peptide were motivated by the fact that the binding motifs of the phosphopeptides are defined by five to six amino acid residues and that short peptide ligands form complexes with 14-3-3ε. Upon sequential truncation (Table S1) of the 14 residue peptide pT, its 9 residues peptide analog pT(501−510) still formed a complex with RMSD (Figure 2A) that is comparable to that of pT.[24] We confirmed the binding of the peptide to 14-3-3ε using DSF, a method that is used to determine the melting temperature of the protein. DSF relies on extrinsic fluorescence-like dyes that allow us to monitor the melting of protein on heating protein solution at increasing temperatures. Ligand binding causes a shift in the melting temperature of the protein.[59] DSF and SPR showed that compared to pT, pT(502−510) caused a larger ΔT_m of 14-3-3ε, and its affinity was ∼3 fold higher than that of pT (Table 2). This improvement in binding affinity may be attributed to the short peptide fitting in the binding groove of 14-3-3ε better than that of the pT peptide. Thus, we introduced various substitutions in the sequence of pT(502−510) to improve its binding to 14-3-3ε (Tables 1 and S2).

To target interaction with 14-3-3ε, we specifically introduced aromatic and positively charged amino acid residues to target interactions such as $\pi-\pi$, anion$-\pi$, cation$-\pi$, and ionic interactions[46,47] between the peptide and 14-3-3ε. Substitution of Gly in position 510 of the peptide with aromatic amino acid residues resulted in favorable modifications (Table 1). The free energy of binding (ΔG_b) obtained by SMD and subsequent US simulations further showed that these modifications resulted in peptides that are more favorably bound to 14-3-3ε than pT(502−510) (Figure 4E). This suggests that aromatic amino acid residues in the peptide analogs could induce weakly polar interactions with amino acid residues of 14-3-3ε (Figure 3). We also introduced Ala and Val at position 510 to ascertain whether the improvement in the binding of the peptide analogs containing the aromatic amino acid residues is due to hydrophobicity or aromaticity. The calculated $\Delta\Delta G_b$ by FoldX for these substitutions was not favorable (Table 1), which was most likely due to a limited number of structural samples. Therefore, we performed SMD and subsequent US simulations for the analogs. Results showed that they both favorably bound 14-3-3ε, but ΔG_b of Ala-substituted analogue was more negative than that of Val. Furthermore, ΔG_b of Ala^{510} containing peptide was comparable to that of the peptides containing aromatic amino acid residues (Figure 4E). These results indicate that aromatic and small hydrophobic amino acid residues are the most suitable in position 510 of the pT(502−510) peptide. Structural features of the peptide analogs determined by DSSP analysis of the 500 ns simulations and those obtained by ECD measurements indicate that the peptides upon binding do not undergo major structural transition. This implies that peptide binding to 14-3-3ε is not opposed by the conformational entropy change of peptides. Although the [Tic^{510}]pT(502−510) peptide in 70% TFE solution had a tendency to adopt a small fraction of helicity (Table S3), none of the other peptides did; therefore, adoption of helicity is not a factor for improvement in binding.

DSF measurements showed that all of the designed peptides caused a shift in T_m of 14-3-3ε. In all melting curves (Figures 6 and S8) of 14-3-3ε, fluorescence increases with the temperature and then decreases at high temperature. The decrease in

https://doi.org/10.1021/acsomega.3c07740
ACS Omega 2024, 9, 2719−2729

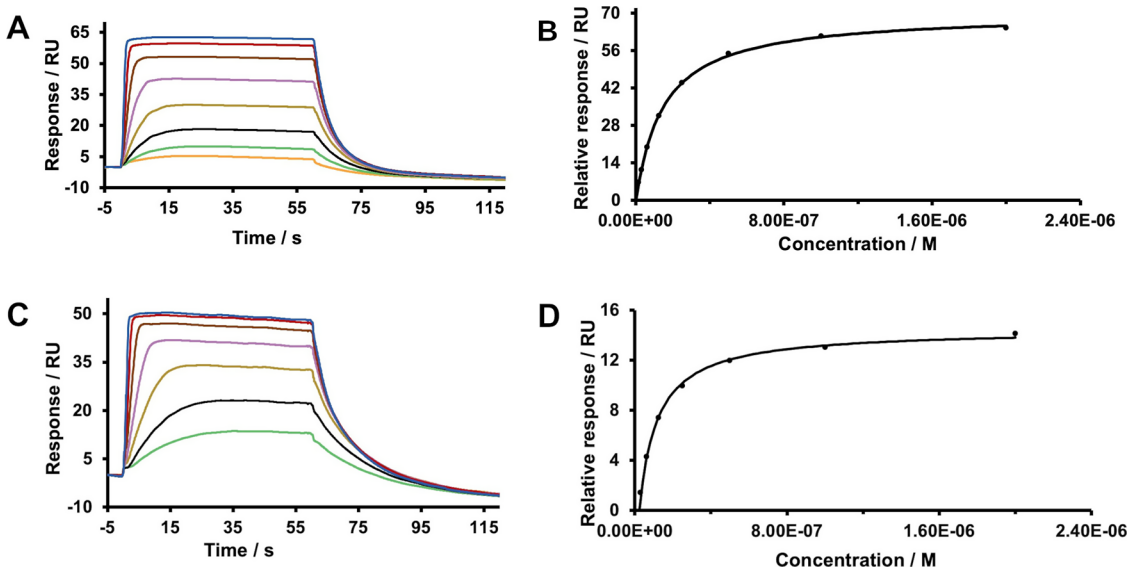

Figure 7. Binding of peptide ligands to 14-3-3ε by surface plasmon resonance (SPR). Sensogram and binding isotherm of 14-3-3ε−pT (A,B) and 14-3-3ε−pT(502−510) and (C,D) complexes. 14-3-3ε was immobilized on sensor chip and the binding of peptides at different concentrations (1−2000 nM) were measured at 298 K. Steady state affinities of the peptides (K_D) were determined using Biacore analysis software.

fluorescence signal at elevated temperature is most likely due to protein aggregation and/or dye dissociation from the protein at high temperatures. As determined by SPR, the [Phe^{510}]pT(502−510) peptide has the highest affinity, ∼6.5 fold higher than that of the pT peptide (Table 2). This implies that the aromatic side chain of Phe fits best in position 510 of pT(502−510). Given the flexibility of the x^1 angle of Phe (Figure S6A), the Gly^{510} was substituted with the Tic amino acid residue to improve conformational stability of the aromatic side chain of Phe^{510}. Currently, no CHARMM36m force field parameters are available for Tic amino acid. Thus, no MD simulations were performed for the [Tic^{510}]pT(502−510)−14-3-3ε complex. However, DSF measurement showed that the peptide caused a significant increase of T_m of 14-3-3ε and the K_D (36.66 nM) of the peptide for the protein, determined by SPR, is comparable to that of [Phe^{510}]pT(502−510) (22.0 nM). Hence, constraining the χ^1 torsional angle of the Phe residue did not improve further the binding affinity. Based on these results, all modification introduced in pT(502−510) improved its binding except the Val^{510} modification, and [Phe^{510}]pT(502−510) is the best peptide candidate for 14-3-3ε (Table 2). Our results are in agreement with the large-scale screening for peptide binding motifs for 14-3-3 isoforms that showed that Phe is the most favorable amino acid residue in position 510 of the peptide motif for 14-3-3ε isoform[10].

5. CONCLUSIONS

In this work, a combination of in silico and biophysical approaches were used to design pT peptide analogs, and studied their binding to 14-3-3ε. Since it is known that short peptide ligands bind 14-3-3ε, we shortened the pT peptide from 14 to 9 amino acid residues (pT(502−510)). SMD studies indicated favorable binding of pT(502−510) to 14-3-3ε, and SPR and DSF showed that pT(502−510) is a stronger binder of 14-3-3ε than pT. Aromatic amino acid residues are involved in various types of interactions; thus, to further improve binding of pT(502−510), we substituted Gly^{510} within pT(502−510) with aromatic amino acid residues. SMD and subsequent US simulations indicated that aromatic amino acid substitutions of the Gly^{510} residue were the most favorable modifications. The simulation results are agreement with both DSF and SPR measurements. All of the studies indicated that the [Phe^{510}]pT(502−510) peptide is the best binder of 14-3-3ε. Our study also highlights the importance of aromatic amino acid residues in interactions of our peptides with 14-3-3ε. Overall, we have designed peptides that bind 14-3-3ε with nanomolar affinities. The shortened peptides could have improved proteolytic stability since several basic residues were removed from the C-terminal end of the parent peptide. The ability of the optimized peptides to induce apoptosis of cSCC cells will be determined in future studies.

■ ASSOCIATED CONTENT

Supporting Information

The Supporting Information is available free of charge at https://pubs.acs.org/doi/10.1021/acsomega.3c07740.

Method for protin expression; Figures S1−S3, detailed analysis of MD simualtions; Figure S5, characterization of SMD simulations; Figure S6, conformational features of Phe and Tic amino acid residues; Figure S7, ECD spectra of peptides; Figure S8 and S9, binding of peptides to 14-3-3ε; Tables S1 and S2, sequences of peptides and their calculated change in binding free energy; Table S3, quantitative analysis of ECD spectra of peptides; Table S4, kinetics of peptide binding (PDF)

■ AUTHOR INFORMATION

Corresponding Author

Sándor Lovas − *Department of Biomedical Sciences, Creighton University, Omaha, Nebraska 68178, United States;* orcid.org/0000-0002-5089-5186; Phone: 402-280-5753; Email: slovas@creighton.edu; Fax: 402-280-2690

Authors

Seraphine Kamayirese − *Department of Biomedical Sciences, Creighton University, Omaha, Nebraska 68178, United States*

https://doi.org/10.1021/acsomega.3c07740
ACS Omega 2024, 9, 2719−2729

Sibaprasad Maity − *Department of Biomedical Sciences, Creighton University, Omaha, Nebraska 68178, United States;* Present Address: Process Development, Corden Pharma, Boulder, Colorado 80301, United States
Lynne M. Dieckman − *Department of Chemistry and Biochemistry, Creighton University, Omaha, Nebraska 68178, United States*
Laura A. Hansen − *Department of Biomedical Sciences, Creighton University, Omaha, Nebraska 68178, United States*

Complete contact information is available at: https://pubs.acs.org/10.1021/acsomega.3c07740

Notes

The authors declare no competing financial interest.

■ ACKNOWLEDGMENTS

This work was supported by the National Institutes of Health R01 CA253573-01 and the state of Nebraska LB595 grants. Mass spectral analysis of synthetic peptides were performed by the Mass Spectrometry Core facility as a component of the Auditory Vestibular Technology Core within the Translational Hearing Center at Creighton University, School of Medicine funded by CoBRE Award 5P20GM139762 from the NIH.

■ REFERENCES

(1) Liang, S.; Xu, Y.; Shen, G.; Liu, Q.; Zhao, X.; Xu, Z.; Xie, X.; Gong, F.; Li, R.; Wei, Y. Quantitative Protein Expression Profiling of 14−3-3 Isoforms in Human Renal Carcinoma Shows 14−3-3 Epsilon Is Involved in Limitedly Increasing Renal Cell Proliferation. *Electrophoresis* **2009**, *30* (23), 4152−4162.
(2) Yaffe, M. B.; Rittinger, K.; Volinia, S.; Caron, P. R.; Aitken, A.; Leffers, H.; Gamblin, S. J.; Smerdon, S. J.; Cantley, L. C. The Structural Basis for 14−3-3:Phosphopeptide Binding Specificity. *Cell* **1997**, *91* (7), 961−971.
(3) Jones, D. H.; Ley, S.; Aitken, A. Isoforms of 14−3-3 Protein Can Form Homo- and Heterodimers in Vivo and in Vitro: Implications for Function as Adapter Proteins. *FEBS Lett.* **1995**, *368* (1), 55−58.
(4) Aitken, A.; Howell, S.; Jones, D.; Madrazo, J.; Patel, Y. 14−3-3 α and δ Are the Phosphorylated Forms of Raf-Activating 14−3-3 β and ζ: In Vivo Stoichiometric Phosphorylation in Brain at a Ser-Pro-Glu-Lys Motif. *J. Biol. Chem.* **1995**, *270* (11), 5706−5709.
(5) Yang, X.; Lee, W. H.; Sobott, F.; Papagrigoriou, E.; Robinson, C. V.; Grossmann, J. G.; Sundström, M.; Doyle, D. A.; Elkins, J. M. Structural Basis for Protein−Protein Interactions in the 14−3-3 Protein Family. *Proc. Natl. Acad. Sci. U. S. A.* **2006**, *103* (46), 17237.
(6) Chaudhri, M.; Scarabel, M.; Aitken, A. Mammalian and Yeast 14−3-3 Isoforms Form Distinct Patterns of Dimers in Vivo. *Biochem. Biophys. Res. Commun.* **2003**, *300* (3), 679−685.
(7) Nagy, G.; Oostenbrink, C.; Hritz, J. Exploring the Binding Pathways of the 14−3-3ζ Protein: Structural and Free-Energy Profiles Revealed by Hamiltonian Replica Exchange Molecular Dynamics with Distancefield Distance Restraints. *PLoS One* **2017**, *12* (7), No. e0180633.
(8) Trošanová, Z.; Louša, P.; Kozeleková, A.; Brom, T.; Gašparik, N.; Tungli, J.; Weisová, V.; Župa, E.; Žoldák, G.; Hritz, J. Quantitation of Human 14−3-3ζ Dimerization and the Effect of Phosphorylation on Dimer-Monomer Equilibria. *J. Mol. Biol.* **2022**, *434*, No. 167479.
(9) Obsil, T.; Obsilova, V. Structural Basis of 14−3-3 Protein Functions. *Semin. Cell Dev. Biol.* **2011**, *22* (7), 663−672.
(10) Li, Z.; Tang, J.; Guo, F. Identification of 14−3-3 Proteins Phosphopeptide-Binding Specificity Using an Affinity-Based Computational Approach. *PLoS One* **2016**, *11* (2), No. e0147467.
(11) Brunet, A.; Bonni, A.; Zigmond, M. J.; Lin, M. Z.; Juo, P.; Hu, L. S.; Anderson, M. J.; Arden, K. C.; Blenis, J.; Greenberg, M. E. Akt Promotes Cell Survival by Phosphorylating and Inhibiting a Forkhead Transcription Factor. *Cell* **1999**, *96* (6), 857−868.
(12) Ganguly, S.; Gastel, J. A.; Weller, J. L.; Schwartz, C.; Jaffe, H.; Namboodiri, M. A. A.; Coon, S. L.; Hickman, A. B.; Rollag, M.; Obsil, T.; Beauverger, P.; Ferry, G.; Boutin, J. A.; Klein, D. C. Role of a Pineal CAMP-Operated Arylalkylamine N-Acetyltransferase/14−3-3-Binding Switch in Melatonin Synthesis. *Proc. Natl. Acad. Sci. U. S. A.* **2001**, *98* (14), 8083−8088.
(13) Chen, M.-S.; Ryan, C. E.; Piwnica-Worms, H. Chk1 Kinase Negatively Regulates Mitotic Function of Cdc25A Phosphatase through 14−3-3 Binding. *Mol. Cell. Biol.* **2003**, *23* (21), 7488−7497.
(14) Al-Matouq, J.; Holmes, T.; Hammiller, B.; Tran, N.; Holmes, M.; Freeman, S. C.; Hansen, L. A. Accumulation of Cytoplasmic CDC25A in Cutaneous Squamous Cell Carcinoma Leads to a Dependency on CDC25A for Cancer Cell Survival and Tumor Growth. *Cancer Lett.* **2017**, *410*, 41−49.
(15) Gardino, A. K.; Yaffe, M. B. 14−3-3 Proteins As Signaling Integration Points for Cell Cycle Control and Apoptosis. *Semin. Cell Dev. Biol.* **2011**, *22* (7), 688−695.
(16) Fan, X.; Cui, L.; Zeng, Y.; Song, W.; Gaur, U.; Yang, M. 14−3-3 Proteins Are on the Crossroads of Cancer, Aging, and Age-Related Neurodegenerative Disease. *Int. J. Mol. Sci.* **2019**, *20* (14), 3518.
(17) Yan, Y.; Xu, Y.; Gao, Y.; Zong, Z.; Zhang, Q.; Li, C.; Wang, H. Implication of 14−3-3ε and 14−3-3θ/τ in Proteasome Inhibition-induced Apoptosis of Glioma Cells. *Cancer Sci.* **2013**, *104* (1), 55−61.
(18) Lee, T.-G.; Jeong, E.-H.; Kim, S. Y.; Kim, H.-R.; Kim, H.; Kim, C.-H. Fhit, a Tumor Suppressor Protein, Induces Autophagy via 14−3-3τ in Non-Small Cell Lung Cancer Cells. *Oncotarget* **2017**, *8* (19), 31923−31937.
(19) Teo, Z.; Sng, M. K.; Chan, J. S. K.; Lim, M. M. K.; Li, Y.; Li, L.; Phua, T.; Lee, J. Y. H.; Tan, Z. W.; Zhu, P.; Tan, N. S. Elevation of Adenylate Energy Charge by Angiopoietin-like 4 Enhances Epithelial-Mesenchymal Transition by Inducing 14−3-3γ Expression. *Oncogene* **2017**, *36* (46), 6408−6419.
(20) Xiao, Y.; Lin, V. Y.; Ke, S.; Lin, G. E.; Lin, F.-T.; Lin, W.-C. 14−3-3τ Promotes Breast Cancer Invasion and Metastasis by Inhibiting RhoGDIα. *Mol. Cell. Biol.* **2014**, *34* (14), 2635−2649.
(21) Gong, X.; Yan, L.; Gu, H.; Mu, Y.; Tong, G.; Zhang, G. 14−3-3ε Functions as an Oncogene in SGC7901 Gastric Cancer Cells through Involvement of Cyclin E and P27kip1. *Mol. Med. Rep.* **2014**, *10* (6), 3145−3150.
(22) Liu, T.-A.; Jan, Y.-J.; Ko, B.-S.; Liang, S.-M.; Chen, S.-C.; Wang, J.; Hsu, C.; Wu, Y.-M.; Liou, J.-Y. 14−3-3ε Overexpression Contributes to Epithelial-Mesenchymal Transition of Hepatocellular Carcinoma. *PLoS One* **2013**, *8* (3), No. e57968.
(23) Holmes, T. R.; Al Matouq, J.; Holmes, M.; Sioda, N.; Rudd, J. C.; Bloom, C.; Nicola, L.; Palermo, N. Y.; Madson, J. G.; Lovas, S.; Hansen, L. A. Targeting 14−3-3ε Activates Apoptotic Signaling to Prevent Cutaneous Squamous Cell Carcinoma. *Carcinogenesis* **2021**, *42* (2), 232−242.
(24) Holmes, T. R.; Al-Matouq, J.; Holmes, M.; Nicola, L.; Rudd, J. C.; Lovas, S.; Hansen, L. A. Targeting 14−3-3ε-CDC25A Interactions to Trigger Apoptotic Cell Death in Skin Cancer. *Oncotarget* **2020**, *11* (35), 3267−3278.
(25) Zhang, L.; Chen, J.; Fu, H. Suppression of Apoptosis Signal-Regulating Kinase 1-Induced Cell Death by 14−3-3 Proteins. *Proc. Natl. Acad. Sci. U. S. A.* **1999**, *96* (15), 8511−8515.
(26) Wang, B.; Yang, H.; Liu, Y.-C.; Jelinek, T.; Zhang, L.; Ruoslahti, E.; Fu, H. Isolation of High-Affinity Peptide Antagonists of 14−3-3 Proteins by Phage Display. *Biochemistry* **1999**, *38* (38), 12499−12504.
(27) Petosa, C.; Masters, S. C.; Bankston, L. A.; Pohl, J.; Wang, B.; Fu, H.; Liddington, R. C. 14−3-3ζ Binds a Phosphorylated Raf Peptide and an Unphosphorylated Peptide via Its Conserved Amphipathic Groove*. *J. Biol. Chem.* **1998**, *273* (26), 16305−16310.
(28) Masters, S. C.; Pederson, K. J.; Zhang, L.; Barbieri, J. T.; Fu, H. Interaction of 14−3-3 with a Nonphosphorylated Protein Ligand, Exoenzyme S of Pseudomonas Aeruginosa. *Biochemistry* **1999**, *38* (16), 5216−5221.

(29) Masters, S. C.; Fu, H. 14−3-3 Proteins Mediate an Essential Anti-Apoptotic Signal*. *J. Biol. Chem.* **2001**, *276* (48), 45193−45200.
(30) Zhao, J.; Du, Y.; Horton, J. R.; Upadhyay, A. K.; Lou, B.; Bai, Y.; Zhang, X.; Du, L.; Li, M.; Wang, B.; Zhang, L.; Barbieri, J. T.; Khuri, F. R.; Cheng, X.; Fu, H. Discovery and Structural Characterization of a Small Molecule 14−3-3 Protein-Protein Interaction Inhibitor. *Proc. Natl. Acad. Sci. U. S. A.* **2011**, *108* (39), 16212−16216.
(31) Higo, J.; Kawabata, T.; Kusaka, A.; Kasahara, K.; Kamiya, N.; Fukuda, I.; Mori, K.; Hata, Y.; Fukunishi, Y.; Nakamura, H. Molecular Interaction Mechanism of a 14−3-3 Protein with a Phosphorylated Peptide Elucidated by Enhanced Conformational Sampling. *J. Chem. Inf. Model.* **2020**, *60* (10), 4867−4880.
(32) Künzel, N.; Helms, V. How Phosphorylation of Peptides Affects Their Interaction with 14−3-3η Domains. *Proteins Struct. Funct. Bioinforma.* **2022**, *90* (2), 351−362.
(33) Andrei, S. A.; de Vink, P.; Sijbesma, E.; Han, L.; Brunsveld, L.; Kato, N.; Ottmann, C.; Higuchi, Y. Rationally Designed Semisynthetic Natural Product Analogues for Stabilization of 14−3-3 Protein-Protein Interactions. *Angew. Chem., Int. Ed. Engl.* **2018**, *57* (41), 13470−13474.
(34) Krieger, E.; Vriend, G. New Ways to Boost Molecular Dynamics Simulations. *J. Comput. Chem.* **2015**, *36* (13), 996−1007.
(35) Kutzner, C.; Páll, S.; Fechner, M.; Esztermann, A.; de Groot, B. L.; Grubmüller, H. Best Bang for Your Buck: GPU Nodes for GROMACS Biomolecular Simulations. *J. Comput. Chem.* **2015**, *36* (26), 1990−2008.
(36) Huang, J.; Rauscher, S.; Nawrocki, G.; Ran, T.; Feig, M.; de Groot, B. L.; Grubmüller, H.; MacKerell, A. D. CHARMM36m: An Improved Force Field for Folded and Intrinsically Disordered Proteins. *Nat. Methods* **2017**, *14* (1), 71−73.
(37) Jorgensen, W. L.; Chandrasekhar, J.; Madura, J. D.; Impey, R. W.; Klein, M. L. Comparison of Simple Potential Functions for Simulating Liquid Water. *J. Chem. Phys.* **1983**, *79* (2), 926−935.
(38) Bussi, G.; Donadio, D.; Parrinello, M. Canonical Sampling through Velocity Rescaling. *J. Chem. Phys.* **2007**, *126* (1), No. 014101.
(39) Berendsen, H. J. C.; Postma, J. P. M.; van Gunsteren, W. F.; DiNola, A.; Haak, J. R. Molecular Dynamics with Coupling to an External Bath. *J. Chem. Phys.* **1984**, *81* (8), 3684−3690.
(40) Hess, B.; Bekker, H.; Berendsen, H. J. C.; Fraaije, J. G. E. M. LINCS: A Linear Constraint Solver for Molecular Simulations. *J. Comput. Chem.* **1997**, *18* (12), 1463−1472.
(41) Parrinello, M.; Rahman, A. Polymorphic Transitions in Single Crystals: A New Molecular Dynamics Method. *J. Appl. Phys.* **1981**, *52* (12), 7182−7190.
(42) Karplus, M.; Kushick, J. N. Method for Estimating the Configurational Entropy of Macromolecules. *Macromolecules* **1981**, *14* (2), 325−332.
(43) Andricioaei, I.; Karplus, M. On the Calculation of Entropy from Covariance Matrices of the Atomic Fluctuations. *J. Chem. Phys.* **2001**, *115* (14), 6289−6292.
(44) Daura, X.; Gademann, K.; Jaun, B.; Seebach, D.; van Gunsteren, W. F.; Mark, A. E. Peptide Folding: When Simulation Meets Experiment. *Angew. Chem., Int. Ed.* **1999**, *38* (1−2), 236−240.
(45) Kabsch, W.; Sander, C. Dictionary of Protein Secondary Structure: Pattern Recognition of Hydrogen-Bonded and Geometrical Features. *Biopolymers* **1983**, *22* (12), 2577−2637.
(46) Palermo, N. Y.; Csontos, J.; Owen, M. C.; Murphy, R. F.; Lovas, S. Aromatic-Backbone Interactions in Model α-Helical Peptides. *J. Comput. Chem.* **2007**, *28* (7), 1208−1214.
(47) Körtvélyesi, T.; Murphy, R. F.; Lovas, S. Secondary Structures and Intramolecular Interactions in Fragments of the B-Loops of Naturally Occurring Analogs of Epidermal Growth Factor. *J. Biomol. Struct. Dyn.* **1999**, *17* (2), 393−407.
(48) Schymkowitz, J.; Borg, J.; Stricher, F.; Nys, R.; Rousseau, F.; Serrano, L. The FoldX Web Server: An Online Force Field. *Nucleic Acids Res.* **2005**, *33*, W382−W388.
(49) Rasafar, N.; Barzegar, A.; Mehdizadeh Aghdam, E. Structure-Based Designing Efficient Peptides Based on P53 Binding Site Residues to Disrupt P53-MDM2/X Interaction. *Sci. Rep.* **2020**, *10* (1), 11449.
(50) Ngo, S. T.; Vu, K. B.; Bui, L. M.; Vu, V. V. Effective Estimation of Ligand-Binding Affinity Using Biased Sampling Method. *ACS Omega* **2019**, *4* (2), 3887−3893.
(51) Wingbermühle, S.; Schäfer, L. V. Capturing the Flexibility of a Protein−Ligand Complex: Binding Free Energies from Different Enhanced Sampling Techniques. *J. Chem. Theory Comput.* **2020**, *16* (7), 4615−4630.
(52) Hub, J. S.; de Groot, B. L.; van der Spoel, D. G_wham—A Free Weighted Histogram Analysis Implementation Including Robust Error and Autocorrelation Estimates. *J. Chem. Theory Comput.* **2010**, *6* (12), 3713−3720.
(53) Kumar, S.; Rosenberg, J. M.; Bouzida, D.; Swendsen, R. H.; Kollman, P. A. THE Weighted Histogram Analysis Method for Free-Energy Calculations on Biomolecules. I. The Method. *J. Comput. Chem.* **1992**, *13* (8), 1011−1021.
(54) Whitmore, L.; Wallace, B. A. DICHROWEB, an Online Server for Protein Secondary Structure Analyses from Circular Dichroism Spectroscopic Data. *Nucleic Acids Res.* **2004**, *32*, W668−673.
(55) Whitmore, L.; Wallace, B. A. Protein Secondary Structure Analyses from Circular Dichroism Spectroscopy: Methods and Reference Databases. *Biopolymers* **2008**, *89* (5), 392−400.
(56) Babula, J. J.; Liu, J.-Y. Integrate Omics Data and Molecular Dynamics Simulations toward Better Understanding of Human 14−3-3 Interactomes and Better Drugs for Cancer Therapy. *J. Genet. Genomics* **2015**, *42* (10), 531−547.
(57) Lovas, S.; Murphy, R. F. Solvated Structure Analysis of a Conformationally Restricted Analogue of Phenylalanine in a Dipeptide Model by the AM1-SM2Method. *J. Mol. Struct.* **1994**, *311*, 297−304.
(58) Chen, Y.-H.; Yang, J. T.; Martinez, H. M. Determination of the Secondary Structures of Proteins by Circular Dichroism and Optical Rotatory Dispersion. *Biochemistry* **1972**, *11* (22), 4120−4131.
(59) Gao, K.; Oerlemans, R.; Groves, M. R. Theory and Applications of Differential Scanning Fluorimetry in Early-Stage Drug Discovery. *Biophys. Rev.* **2020**, *12* (1), 85−104.

https://doi.org/10.1021/acsomega.3c07740
ACS Omega 2024, 9, 2719−2729